Transactions of the Materials Research Society of Japan 32[4] 1231-1234 (2007)

Fabrication of Magnetoelectric Cr_2O_3 Films for Application Single Flux Quantum Device

Takeshi Asada, Kenjirou Nagase, Takayuki Yamada, Nobuyuki Iwata and Hiroshi Yamamoto
College of Science & Technology Nihon University (CST), 7-24-1 Narashinodai, Funabashi-shi, Chiba 274-8501
Fax: +81-47-469-5457, e-mail: 2005_asada@yamanoya.ecs.cst.nihon-u.ca.jp

Thin films of magnetoelectric (ME) materials are expected to be applied to novel superconducting devices as voltage-controlled magnetic/current sources and gates. As a representative ME material Cr_2O_3 films were prepared on *R*-cut sapphire substrates by *DC-RF* hybrid magnetron sputtering. Strong Bragg diffraction peaks (n 0 -n 2n) from Cr_2O_3 with a trigonal phase were observed. Then full width at half maximum of rocking curves of (10-12) was 0.58degrees in the film deposited on substrate of 500°C substrates. The surface morphology of the film prepared at 550°C was very smooth with a step and terrace structure. The steps height was same the lattice spacing of Cr_2O_3 (10-12) planes. The Cr_2O_3 films deposited on Nb-$SrTiO_3$ (100) with CeO_2 buffer layers revealed *a*-axis or *c*-axis oriented growth. The CeO_2 buffer layer proceeded the growth of Cr_2O_3. A leakage current through the Cr_2O_3 film was suppressed less than $10^{-5}A/cm^2$ below the electric field of 0.24MV/cm.

Key words: magnetoelectric effect, Cr_2O_3, Nb-STO, CeO_2 buffer, epitaxial growth

1. INTRODUCTION

A magneto-electric effect is defined as an appearance of magnetic fields induced by electric fields. When electric fields are applied, the deviation of ±ions in the crystal takes place and results in changes of magnetic superexchange interactions and magnetic fields appear outside [1,2]. As a representative ME material antiferromagnetic insulator Cr_2O_3 has been studied [3]. Since magnetic fields are induced along the direction of electric fields applied, the orientation and crystallinity of the ME material are determining factors

It is expected that thin films of ME materials are applied to novel superconducting Josephson devices with voltage-control type of magnetic or current sources and gates. Fig. 1. shows the schematic example of a single flux quantum (SFQ) device fabricated by both cuprate high temperature superconductors (HTS) and ME thin films. When electric fields are applied to the ME thin film, magnetic fields are induced to generate shielding current in the superconductor loop including Josephson junctions. The novel circuit element enables a dispersed current source system for highly integrated SFQ circuits and also improves the performance of 100GHz class of high speed SFQ switching.

Most of HTS circuits have been prepared on cubic perovskite substrates, $SrTiO_3$(STO) or MgO. A crystal matching is not good between the substrate crystal and the trigonal Cr_2O_3. Cr_2O_3 films should be deposited on STO substrates buffered by cubic CeO_2 which has been studied for preparation of HTS thin films [4-7]. The purposes of this work are to optimize the substrate temperature for sputtered Cr_2O_3 films on *R*-cut sapphire (10-12) and to investigate the film growth on Nb-$SrTiO_3$ (STO) with CeO_2 buffer layers.

2. EXPERIMENTAL

Cr_2O_3 films were deposited by off-axis *DC-RF* hybrid magnetron sputtering from a Cr metal target with the diameter of two-inch [8]. The typical growth conditions were as follow: substrate temperature (*Ts*) of 300~600°C, *DC* current of 0.04 A, *RF* power of 100 W and sputtering pressure of 0.26 Pa ($Ar:O_2$=4:1).

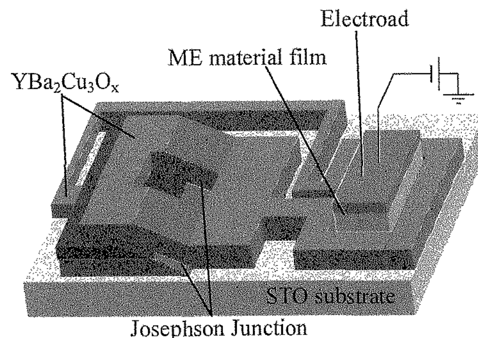

Fig. 1. Schematic novel HTS SFQ circuit as an application of ME material. Magnetic fields induced from the ME film generates base or shielding current in the Josephson junctions loop.

Substrates of *R*-cut sapphire single crystals (5 × $10mm^2$) were etched by HF($HF:H_2O$=1:7) for 10 s before annealing at 1000°C for 12 hour in the air.

As a substrate, CeO_2 buffer layer was deposited by off-axis *RF* magnetron sputtering on Nb-STO(Nb 0.5wt%dope) and post-annealed at 500 or 1000°C in the air. Several CeO_2//Nb-STO substrates with different average roughness (*R*a) were obtained and compared with the results for the Cr_2O_3 films growth.

The crystalline structure of the films was analyzed by X-ray diffraction (XRD: Rigaku RAD-C) with 2θ-θ scan from 5 to 90 degrees. Surface morphology was observed by an atomic force microscopy (AFM: Seiko Instruments Inc. Nanonavi-station).

3. RESULTS & DISCUSSION

3.1 Growth of Cr_2O_3 thin film on the *R*-cut sapphire

Fig. 2. shows the XRD pattern of Cr_2O_3//*R*-cut sapphire prepared at *Ts*=500°C. The open-circles peaks show the peaks from the sapphire substrate. All Bragg diffraction peaks were assigned to *R*-plane (n 0 –n 2n) of trigonal Cr_2O_3 phase and the substrate. The lattice spacing evaluated from the Cr_2O_3 (10-12) peak was 0.363nm same to that of bulk crystal. Fig. 3. shows the enlarged (10-12) peaks of the films deposited at *Ts*=300～600°C. Crystallization of the trigonal Cr_2O_3 phase was confirmed at *Ts*'s above 300°C.

Fig. 4. shows the full width at half maximum (FWHM) of Cr_2O_3 (10-12) rocking curve. The smallest FWHM was 0.58 degrees in the film prepared at *Ts*=500°C, which revealed the superior crystal growth.

Since the inplane lattice parameter of *R*-planes of Cr_2O_3 is larger by about 4% than that of *R*-cut sapphire. The lattice spacing of Cr_2O_3 films are contracted in planes by internal compressive stress and are expanded perpendicular to substrate planes by tensile stress.

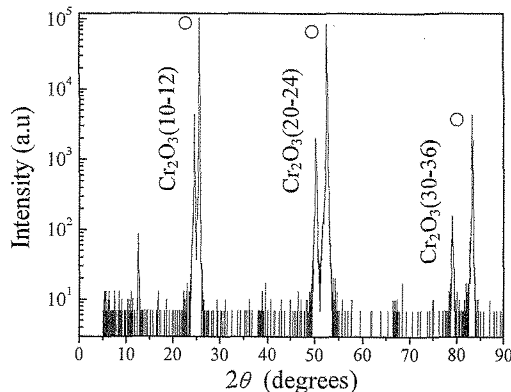

Fig. 2. XRD pattern of Cr_2O_3 film deposited on *R*-cut sapphire at *Ts*=500°C. Open circles show Bragg peaks from the substrate.

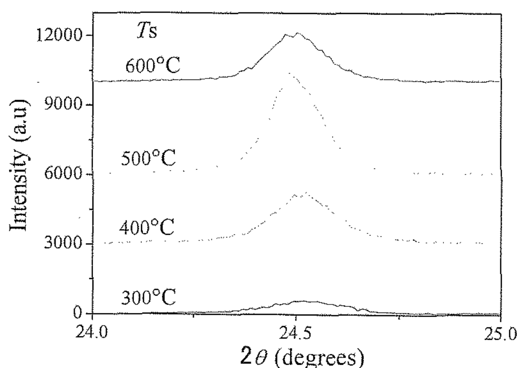

Fig. 3. Cr_2O_3 (10-12) Bragg peaks were observed in the films prepared on *R*-cut sapphire at *Ts*=300°C～600°C. The peak of the film deposited at 500°C was large and sharp.

From the results of XRD it was found that the lattice spacing of the film at *Ts*=500℃ was almost same to that of the bulk and the internal stress was relieved.

Fig. 5. shows AFM surface images and line-profiles of Cr_2O_3 films prepared at various *Ts*'s. In (a-1) at

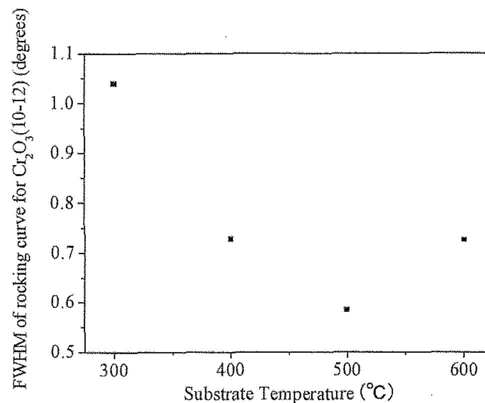

Fig. 4. FWHM of Cr_2O_3 (10-12) rocking curves of the films vs. *Ts*. The minimum value observed was 0.58degrees at *Ts*=500℃.

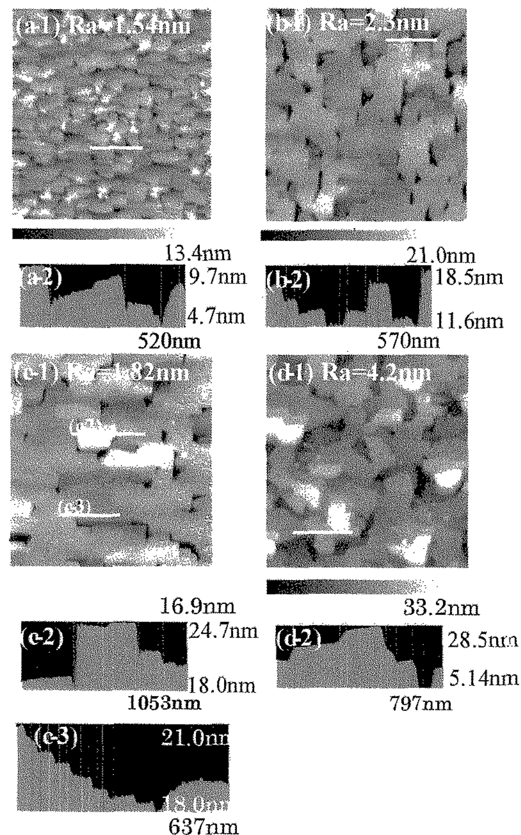

Figure 5. AFM surface images ($2\times2\mu m^2$) and line-profiles of Cr_2O_3 thin films prepared at *Ts*= 400℃ (a-1 and 2), 500℃ (b-1 and 2), 550℃ (c-1, 2 and 3), 600℃ (d-1 and 2).

Ts=400°C, characteristic rectangle grains appeared with the size 100×100~200nm^2. From the line-profile (a-2), the average bump between grains was approximately 3.5nm. The average roughness (Ra) was comparatively small, 1.5nm. In (b-1) at *Ts*=500°C, the grains coalesced and their shape changed into square. In (c-1) at *Ts*=550°C, the coalescence proceeded more clearly and grain boundaries decreased. As shown in the focused line-profile (c-3) several steps were clearly observed in one grain plane. Those steps height was same the lattice spacing of Cr_2O_3 with *R*-plane (0.363nm). The surface morphology suggested the 2-dimensional growth took place on 550°C substrates. In (d-1) at *Ts*= 600°C, the grain size became larger. The bump of grains increased as increasing *Ts*. The value of *R*a was large, 4.2nm and bunching steps increased. A step and terrace structure disappeared as shown in (d-2).

It is thought that the grain boundary is caused by the internal stress which is induced from the lattice mismatch. As stated in the XRD result the inplane stress from the *R*-cut sapphire was relieved at about 500°C. The surface of the film prepared at the 550°C was very smooth and revealed 2-dimensional growth. Conclusively the results of XRD and AFM suggested that the growth of Cr_2O_3 is superior at *Ts*=500~550°C and results in an excellent step and terrace structure which suggests the possibility of an epitaxial growth.

3.2 Growth of Cr_2O_3 on the Nb-STO with CeO_2 buffer

Cr_2O_3 films were not grown directly on the STO substrate. Then the buffer layers of CeO_2 were prepared. Fig. 6. shows XRD patterns of Cr_2O_3/CeO_2//Nb-STO bi-layers (sample A, B and C). The sample A was deposited on the rough CeO_2 layer which was not post-annealed after sputter deposition and has *Ra*=4.2nm. No Bragg diffraction peak from Cr_2O_3 was observed. The sample B was prepared on the smooth CeO_2 @*Ra*=0.41nm layer, post-annealed at 1000°C. The sample revealed a *c*-axis oriented growth of the trigonal Cr_2O_3. The sample C was deposited on the CeO_2 layer post-annealed at 500°C and showed mixed phase growth with *a*-axis orientation. The Cr_2O_3 (n n -2n 0) and (30-30) peaks were observed. The results of XRD indicated that the trigonal Cr_2O_3 grew on the CeO_2 (100)//STO(100) with *a*-axis or *c*-axis orientation.

The AFM surface images of sample A and B were shown in Figures 7(a-1) and (b-1). Figures 7(a-2) and (b-2) show the surface morphology of the CeO_2 (100) substrate for sample A and B, respectively. In the film (a-1) grown on the substrate (b-1) various sizes of grains and deep valleys of grain boundaries were observed. The depth of the valley was above 70nm and the value of *R*a was ca. 17nm. In the film (b-1) on the substrate (b-2) smooth surfaces with *R*a of 4.2nm were observed.

The surfaces of sample A were not smooth and no Bragg diffraction peak was observed. On the other hand, hexagonal grains appeared in smooth surfaces of sample B. So it was thought that the smooth part of sample B corresponded to *c*-planes of Cr_2O_3. These results suggested that the smoothness of the CeO_2 layer affected to Cr_2O_3 growth as a dominant factor and applications of Cr_2O_3 films are fulfilled for SFQ electronic devices fabricated on STO substrates.

Fig. 8. shows a leakage current density as a function of applied electric field in sample B. The diameter of the measuring electrode was 0.45mm and the total thickness of the Cr_2O_3/CeO_2 film was *ca.* 230nm. The observed leakages current was suppressed less than 10^{-5}A/cm^2 below electric field of 0.24MV/cm, the applied voltage of about 5V. So the Cr_2O_3 film works as the ME material under the order of 0.1MV/cm.

Assuming that the ME coefficient of Cr_2O_3 along the

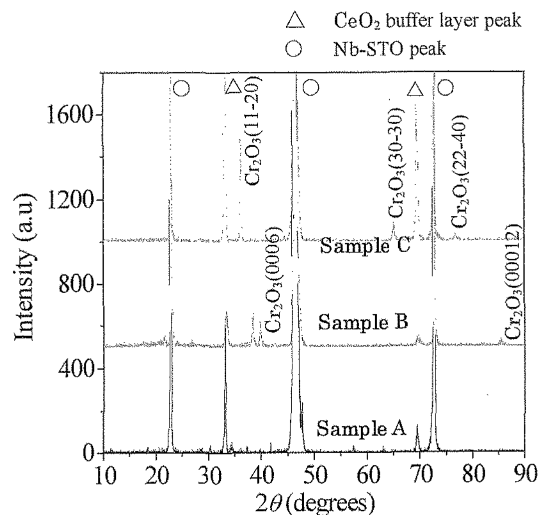

Fig. 6. XRD patterns of Cr_2O_3/CeO_2// Nb-STO sample A, B, and C. The preferential *c*-axis orientation was confirmed in sample B. Sample C shows the *a*-axis growth with (n n –2n 0) plane.

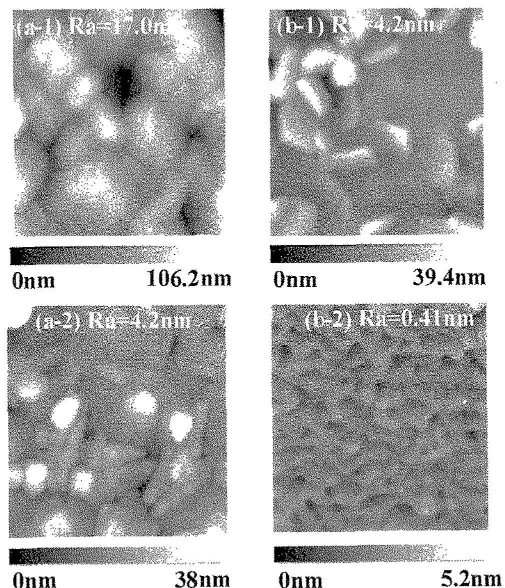

Fig. 7. AFM surface images (1×1 μ m^2) of sample A (a-1) , sample B (b-1), the CeO_2//Nb-STO substrate of sample A (a-2), and the substrate of sample B (b-2).

c-axis is 10^{-4} at about 50K [9, 10], the expected magnetic field in the film is about 1Gauss. Also the magnetic field induced at 300K attains up to 10Gauss, ten times as large as that at 50K.

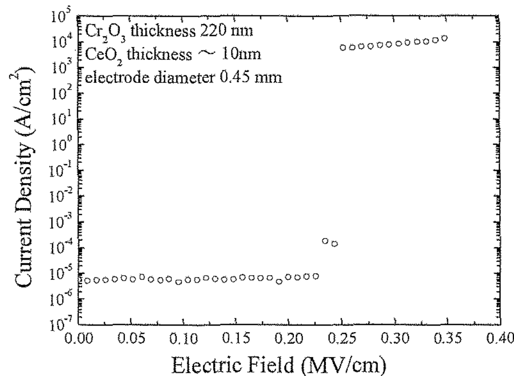

Fig. 8. The leakage current density vs. applied electric field in sample B of Cr_2O_3/CeO_2//Nb-STO. The bi-layered film was an insulator below electric field of *ca.* 0.24MV/cm.

4. CONCULUSION

The ME Cr_2O_3 films were prepared on the *R*-cut sapphire and on Nb-STO with CeO_2 buffers by sputtering. The 2-dimensional growth of Cr_2O_3 was observed on the *R*-cut sapphire at 500~550°C. The CeO_2//Nb-STO substrate successfully resulted in the growth of Cr_2O_3 with *a*-axis and *c*-axis orientation. The prepared Cr_2O_3/CeO_2//Nb-STO revealed the superior insulating properties and assured comparatively large magnetic field of about 1Gauss. The obtained results strongly suggested that the Cr_2O_3 films are applicable for novel SFQ devices fabricated on cubic STO substrates.

5. REFERENCES

[1] K. Siratori, K. Kohn, and E. Kita, *Acta physica polonica A.*, **81**, 431-466 (1992).

[2] P. J. Brown, J. B. Forsyth, and F. Tasset, *Solid State Science.*, 7, 682-689 (2005).

[3] M. Foebig, *Journal of Physics D*, **38**, 123-152 (2005).

[4] M. Shirakawa, M. Miura, T. Ohazama, Y. Shingai, A. Saito, M. Mukaida, and S. Ohshima, *Physica C.*, **412**, 1277-1280 (2004).

[5] M. Spancova, I. Vavra, S Gazi, D. Machajdik, S. Chromik, K. Frohlich, *Journal of Crystal Growth.*, **218**, 287-293 (2000).

[6] H. Y. Lee, S. I. Kim, Y. P. Hong, Y. C. Lee, Y. H. Park, K. H. Ko, *Surface and Coatings Technogy.*, **173**, 224-228 (2003).

[7] Ai. Kamitani, H. Wakana, A. Ogawa, S. Adachi, K. Higuchi, H. Yamamoto, K. Tanabe, *J. Mater. Res.*, **21**, 263-269 (2006).

[8] P. Hones, M. Diserens, F. Levy, *Surface and Coatings Technogy.*, **120**, 277-283 (1999)

[9] H. Wigelmann, A. G. M Jansen, P. River and H. Schmid, *Ferroelectric.*, **62**, 141-146 (1994).

[10] N. Iwata, K. Matso, N. Ootsuka and H. Yamamoto, *Mat. Res. Soc. Symp. Proc.*, **811**, 425-430 (2004).

(Received December 10, 2006;Accepted August 21, 2007)